Brief Communication

MOLECULAR METABOLISM

Metabolic syndrome and extensive adipose tissue inflammation in morbidly obese Göttingen minipigs

Simone Renner [1,2,3,*,19], Andreas Blutke [4,19], Britta Dobenecker [5], Georg Dhom [1,2], Timo D. Müller [3,6,7], Brian Finan [3,6,7], Christoffer Clemmensen [3,6,7], Maren Bernau [8], Istvan Novak [1,2], Birgit Rathkolb [1,2,9], Steffanie Senf [10], Susanne Zöls [10], Mirjam Roth [11], Anna Götz [6,12], Susanna M. Hofmann [3,13,14], Martin Hrabě de Angelis [3,9,15], Rüdiger Wanke [4], Ellen Kienzle [5], Armin M. Scholz [8], Richard DiMarchi [16,17], Mathias Ritzmann [10], Matthias H. Tschöp [3,6,7], Eckhard Wolf [1,2,3,18]

ABSTRACT

Objective: The worldwide prevalence of obesity has increased to 10% in men and 15% in women and is associated with severe comorbidities such as diabetes, cancer, and cardiovascular disease. Animal models of obesity are central to experimental studies of disease mechanisms and therapeutic strategies. Diet-induced obesity (DIO) models in rodents have provided important insights into the pathophysiology of obesity and, in most instances, are the first in line for exploratory pharmacology studies. To deepen the relevance towards translation to human patients, we established a corresponding DIO model in Göttingen minipigs (GM).

Methods: Young adult female ovariectomized GM were fed a high-fat/high-energy diet for a period of 70 weeks. The ration was calculated to meet the requirements and maintain body weight (BW) of lean adult minipigs (L-GM group) or increased stepwise to achieve an obese state (DIO-GM group). Body composition, blood parameters and intravenous glucose tolerance were determined at regular intervals. A pilot chronic treatment trial with a GLP1 receptor agonist was conducted in DIO-GM. At the end of the study, the animals were necropsied and a biobank of selected tissues was established.

Results: DIO-GM developed severe subcutaneous and visceral adiposity (body fat >50% of body mass vs. 22% in L-GM), increased plasma cholesterol, triglyceride, and free fatty acid levels, insulin resistance (HOMA-IR >5 vs. 2 in L-GM), impaired glucose tolerance and increased heart rate when resting and active. However, fasting glucose concentrations stayed within normal range throughout the study. Treatment with a long-acting GLP1 receptor agonist revealed substantial reduction of food intake and body weight within four weeks, with increased drug sensitivity

[1]Chair for Molecular Animal Breeding and Biotechnology, Gene Center and Department of Veterinary Sciences, LMU Munich, Feodor-Lynen-Str. 25, 81377, Munich, Germany [2]Center for Innovative Medical Models (CiMM), Department of Veterinary Sciences, LMU Munich, Hackerstr. 27, 85764, Oberschleißheim, Germany [3]German Center for Diabetes Research (DZD), Ingolstädter Landstr. 1, 85764, Neuherberg, Germany [4]Institute of Veterinary Pathology, Center for Clinical Veterinary Medicine, LMU Munich, Veterinärstr. 13, 80539, Munich, Germany [5]Chair of Animal Nutrition and Dietetics, Department of Veterinary Sciences, LMU Munich, Schönleutnerstr. 8, 85764, Oberschleißheim, Germany [6]Institute for Diabetes and Obesity (IDO), Helmholtz Diabetes Center, Helmholtz Zentrum München, German Research Center for Environmental Health (GmbH), Ingolstädter Landstr. 1, 85764, Neuherberg, Germany [7]Division of Metabolic Diseases, Department of Medicine, Technische Universität, Ismaninger Str. 22, 81675, Munich, Germany [8]Livestock Center of the Veterinary Faculty, LMU Munich, St.-Hubertus-Str. 12, 85764, Oberschleißheim, Germany [9]German Mouse Clinic (GMC), Institute of Experimental Genetics, Helmholtz Zentrum München, German Research Center for Environmental Health, Ingolstädter Landstr. 1, 85764, Neuherberg, Germany [10]Clinic for Swine, Center for Clinical Veterinary Medicine, LMU Munich, Sonnenstr. 16, 85764, Oberschleißheim, Germany [11]Animal aspects, 88400, Biberach an der Riss, Germany [12]Department of Internal Medicine I, University Hospital RWTH Aachen, Pauwelstr. 30, 52074, Aachen, Germany [13]Institute of Diabetes and Regeneration Research (IDR), Helmholtz Diabetes Center, Helmholtz Zentrum München, German Research Center for Environmental Health (GmbH), Ingolstädter Landstr. 1, 85764, Neuherberg, Germany [14]Medizinische Klinik und Poliklinik IV, Klinikum der LMU, Ziemssenstr, 180336, Munich, Germany [15]Genome Analysis Center (GAC), Institute of Experimental Genetics, Helmholtz Zentrum München, German Research Center for Environmental Health and Chair of Experimental Genetics, Technische Universität, Ingolstädter Landstr. 1, 85764, Neuherberg, Germany [16]Novo Nordisk Research Center Indianapolis, 5225 Exploration Drive, Indianapolis, IN, 46241, USA [17]Department of Chemistry, Indiana University, 800 E. Kirkwood Ave., Bloomington, IN, 47405-7102, USA [18]Laboratory for Functional Genome Analysis (LAFUGA), Gene Center, LMU Munich, Feodor-Lynen-Str. 25, 81377, Munich, Germany

[19] Simone Renner and Andreas Blutke contributed equally to this work.

*Corresponding author. CiMM, Hackerstr. 27, 85764, Oberschleißheim, Germany. E-mail: simone.renner@lmu.de (S. Renner).

Abbreviations: AD, apparent digestibility; Aib, aminoisobutyric acid; ALT, alanine-aminotransferase; AD, apparent digestibility; AST, aspartate-aminotransferase; BW, body weight; Cex, C-terminal extended; D, digestibility; DE, digestible energy; DIO, diet-induced obesity; DM, dry matter; DXA, dual-energy X-ray absorptiometry; FBS, fasting blood sampling; FI, food intake; FW, feeding week; GE, gross energy; GFR, glomerular filtration rate; GGT, gamma-glutamyl transferase; GLP1, glucagon-like peptide 1; GLP1R, GLP1 receptor; GM, Göttingen minipig; HE, hematoxylin eosin; HFHE, high-fat/high-energy; kg, kilogram; HR, heart rate; IVGTT, intravenous glucose tolerance test; L, lean; LPS, lipopolysaccharide; MRT, magnetic resonance tomography; ROS, reactive oxygen species; RPAW, retroperitoneal adipose tissue of the abdominal wall; SAT, subcutaneous adipose tissue; S.C., subcutaneous; TAT, total adipose tissue; TT, treatment trial; VAT, visceral adipose tissue; VISC, visceral

Received April 22, 2018 • Revision received June 16, 2018 • Accepted June 25, 2018 • Available online 28 June 2018

https://doi.org/10.1016/j.molmet.2018.06.015

MOLECULAR METABOLISM

relative to observations in other DIO animal models. Extensive adipose tissue inflammation and adipocyte necrosis was observed in visceral, but not subcutaneous, adipose tissue of DIO-GM.

Conclusions: The Munich DIO-GM model resembles hallmarks of the human metabolic syndrome with extensive adipose tissue inflammation and adipocyte necrosis reported for the first time. DIO-GM may be used for evaluating novel treatments of obesity and associated comorbidities. They may help to identify triggers and mechanisms of fat tissue inflammation and mechanisms preventing complete metabolic decompensation despite morbid obesity.

Keywords Pig; High fat diet; Obesity; Diabetes; Metabolic syndrome; Adipose tissue inflammation

1. INTRODUCTION

The prevalence of obesity is persistently increasing worldwide, and the magnitude has nearly doubled in more than 70 countries since 1980. In 2015, approximately 604 million adults were considered obese [1]. Visceral obesity is associated with numerous adverse metabolic effects, including insulin resistance [2], dyslipidemia [3], and hypertension [4]. Obese individuals are susceptible to co-morbidities such as type 2 diabetes mellitus [5], nonalcoholic fatty liver disease (NAFLD) and steatohepatitis [6], asthma [7], certain cancers [8], and cardiovascular [9] and neurodegenerative diseases [10]. The clustered hallmarks of the metabolic syndrome (hyperglycemia, hypercholesterolemia, hypertension and obesity) are major risk factors for cardiovascular disease [11].

Persistent positive energy balance leads to hypersecretion of insulin and catecholamines as well as fat accumulation. It occurs mainly in classical subcutaneous and visceral fat depots but also at multiple other sites like lung, blood vessel wall, epicardium, kidney and bone marrow [12]. While visceral fat depots are closely linked to metabolic disease, subcutaneous fat depots are protective [13].

In adipocytes, excessive fat storage initiates an inflammatory stress response characterized by the secretion of a large variety of chemokines (reviewed in [14]). Although the initial inflammatory response seems to be necessary for acute, physiological fat tissue expansion [15], chronic and centralized, low-grade inflammation triggers insulin resistance. It is accompanied by adipocyte death, abnormal fat tissue remodeling and fibrosis in rodents [16] and humans [17].

To date the metabolic consequences of excessive fat storage are well understood, but the actual triggers and underlying mechanisms of adipose tissue inflammation are uncertain [18]. A deeper understanding of inflammatory triggers and mechanisms may uncover novel therapeutic targets for treatment of obesity and associated comorbidities.

In this respect, animal models that manifest critical disease aspects of human obesity and co-morbidities are important for increasing our knowledge of pathological processes and assessment of drug candidates for translation to human subjects. Diet-induced obese (DIO) rodent models are most often the first-line option for pharmacological evaluation, but their predictive value for drug efficacy and safety in humans is limited [19,20]. Given the strong similarity of human anatomy and physiology to pigs, they can serve as a model bridging the gap between mouse and man [20,21].

Therefore, we have established a DIO model in Göttingen minipigs (GM) to complement a well-characterized DIO mouse model [22,23]. Munich DIO-GM showed phenotypic signatures representative of the metabolic syndrome, as well as extensive fat tissue inflammation. A biobank of selected tissues from DIO-GM and lean controls (L-GM) was established for future molecular profiling studies aimed at the discovery of biomarker candidates and therapeutic targets.

2. MATERIAL AND METHODS

2.1. Animals and study outline

Twenty-six female Göttingen minipigs (GM), 11–13 months of age, were purchased from Ellegaard Göttingen Minipigs A/S, Dalmose, Denmark. Pigs were group-housed until central venous catheters were placed, with straw litter and ad libitum access to water. All experiments were performed according to the German Animal Welfare Act with permission from the responsible authority (Government of Upper Bavaria), following the ARRIVE guidelines and Directive 2010/63/EU. Following an acclimatization period of six weeks, pigs were ovariectomized (see Supplemental methods). The study outline is shown in Figure 1A.

2.2. Diet and feeding regimen

The composition of the experimental diet (high-fat/high-energy; HFHE) is outlined in Suppl. Table 1. The animals were randomized into two experimental groups according to their body fat mass (first DXA measurement) in the first and body weight in the second order: lean and obese. Both groups were fed a restricted ration of the same diet once daily. For the lean group (L-GM), the ration was calculated to meet the energy and nutrient requirements of adult pigs [24]. For the obese group (DIO-GM), the daily ration was increased stepwise to achieve a weekly BW gain of 1.0–1.5 kg up to 80 kg BW and 0.5–1.0 kg from 80 to 100 kg BW. From feeding week (FW) 55 onwards, DIO-GM were offered food ad libitum for 1 h in the morning and 1 h in the afternoon (see pilot treatment trial below). Pigs were individually fed throughout the study period and the daily ration was measured for each pig.

2.3. Diet digestibility

The apparent digestibility (aD) of nutrients was determined at FW 20 (DI) and 70 (DII). Titanium oxide (0.1% of dry matter) was added to the food as marker, and feces were collected from each individually housed minipig for a 5-day period. Subsequently, food and feces were freeze-dried, grinded, and mixed thoroughly. Crude nutrients were determined using the Weende method (VDLUFA 2012) and gross energy (GE) using an adiabatic bomb calorimeter. For mineral analysis, wet digestion of feed and fecal samples was performed in a microwave digestion unit (MLS Ethos 1600). Calcium was determined by flame emission spectrometry (EFOX 5053, Eppendorf AG, Hamburg, Germany) and phosphorus photometrically with ammonium molybdate and ammonium vanadate in HNO_3 (GENESYS 10 UV, Thermo Spectronic, Rochester, NY, USA). Using the aD of GE from the balancing trials based on the following equation, digestible energy (DE) intake was calculated:

aD [%] = 100 − [% marker diet/% marker feces × % nutrient feces/% nutrient food] * 100.

2.4. Body weight, body composition and fat distribution

Body weight was determined two (up to FW 54) or three times (treatment trial) per week using an F. Star 125 large animal scale (Meier-Brakenberg). Whole body composition was evaluated by dual-energy X-ray absorptiometry (GE Lunar *i*DXA scanner; GE Healthcare GmbH, Solingen, DE) prior to HFHE feeding (0) as well as in FW 18, 30 and 54 as described in [25]. In addition, magnetic resonance tomography (MRT; Magnetom Open Scanner, 0.2 T, Siemens) was performed in FW 30 using a T1-weighted sequence as described in [26] with a slice thickness = 15 mm, field of view = 461 mm × 461 mm, TR (time of repetition) = 380 ms, and TE (time between echoes) = 15 ms.

2.5. Blood parameters

Blood samples were taken after an overnight fasting period of 18–20 h prior to the start of HFHE feeding (0) and in FW 18, 30, and 54. Blood was collected into EDTA-coated and non-coated tubes (Monovette® blood collection system, Sarstedt). EDTA-plasma tubes were immediately stored on ice, while serum tubes were kept at room temperature for 20 min to allow complete clotting. Then plasma/serum was separated by centrifugation (1,500 × *g*, 4 °C, 15 min), aliquoted and stored at −80 °C. Plasma insulin levels were determined using a species-specific RIA (Merck Millipore). Clinical-chemical parameters were determined from EDTA-plasma or serum (Suppl. Table 2) using an AU480 autoanalyzer (Beckman–Coulter) and adapted reagent kits from Beckman–Coulter or Sentinel. Amylase and lipase were determined using an ILab 650 analyzer (Werfen GmbH) and respective reagent kits.

2.6. Intravenous glucose tolerance test (IVGTT)

For stress-free, frequent blood sampling in unrestrained animals, central venous catheters were placed into a marginal ear vein (Suppl. Methods). IVGTTs were performed in FW 29 and 54 as previously described [27].

2.7. Heart rate

Non-invasive heart rate measurement was performed in FW 59 and 69 using a Zephyr BioHarness 3.0 system (Cosmed) at rest (lying animal) and during a relaxed walk of 1 min duration. Animal behavior was monitored during the entire recording period.

2.8. Pilot treatment trial

Starting at feeding week 60, a pilot pharmacology trial was performed using a long acting GLP1 receptor (GLP1R) agonist in chronic treatment. Eight obese GM (96.4 ± 3.1 kg) were randomized according to body fat mass determined by DXA (FW 54) and body weight to placebo administration (0.9% NaCl) or treatment with a GLP1R agonist (acylated GLP1, i.e. GLP1 [Aib^2 E^{16} Cex K^{40}-C^{16} acyl] [28]). Two weeks prior to treatment start, GM received ad libitum food for 1 h in the morning (08:00–09:00) and 1 h in the afternoon (03:00–04:00). Compound/placebo was subcutaneously injected once daily (between 08:00 and 08:30) into the popliteal crease for a total period of 29 days, twenty days with a dosage of 0.1 μg/kg BW and nine days with 0.2 μg/kg BW. During the treatment period, food intake was recorded once daily, and body weight was recorded three times per week. Animals were continuously monitored for the occurrence of possible gastrointestinal side effects.

2.9. Pathological examination and establishment of a biobank

Following a wash-out period of four weeks for trial participants, all animals were necropsied. Pigs were anesthetized by intramuscular injection of ketamine (Ursotamin®, Serumwerke Bernburg, 20 mg/kg BW) and azaperone (Stresnil®, Elanco, 2 mg/kg BW) followed by intravenous application of ketamine and xylazine (Xylazin 2%, Serumwerk Bernburg). Blood samples were taken by cardio puncture. Animals were then euthanized under anesthesia by intravenous injection of Pentobarbital (Release®, WDT, at least 450 mg/10 kg BW) and immediately subjected to necropsy. Body weight and the weights, dimensions, and densities of internal organs and different defined adipose tissue depots (refer to Suppl. Table 5 and Suppl. Figure 4) were determined, according to standardized tissue sampling guidelines as described previously [29,30]. Samples designated for molecular profiling were shock frozen to −80 °C within a period of 20 min after death of the animal. Tissue samples for histopathological analyses were fixed in neutrally buffered 4% formaldehyde solution and processed for paraffin-histology or cryo-histology according to standard protocols [29]. Transversal sections of formalin-fixed, paraffin-embedded tissue samples of terminal abdominal aorta and of cardiac coronary arteries were stained with HE, giemsa, picrosirius red, and Masson's trichrome. For demonstration of lymph-vessels in paraffin sections of lung tissue, the lymphatic marker protein LYVE1 (lymphatic vessel endothelial hyaluronic acid receptor 1) was detected by immunohistochemistry, using a polyclonal rabbit anti-LYVE1 IgG antibody (1:100, ab 33682, Abcam™, UK), a horse-radish peroxidase-coupled goat anti-rabbit IgG secondary antibody (1:100, P0448, Dako™, Denmark), diaminobenzidine as final chromogen, and hemalum as nuclear counterstain. A biobank collection of samples of >20 different organs, tissues and body fluids was established [29], providing adequately processed specimen for a broad spectrum of subsequent analysis methods, including molecular analyses of RNA, proteins, and metabolites, microbiomic analyses of intestinal contents, as well as qualitative and quantitative morphological analyses on the level of light- and electron microscopy (Supplementary Table 7).

2.10. Determination of adipose tissue necrosis volumes

The excised retroperitoneal adipose tissue of the abdominal wall (rpAW) was cut completely into parallel stripes of tissue approximately two centimeter thickness. The tissue stripes were placed on the same cut-surfaces and photographed vertically from above, together with a ruler. Digital images of the photographs were superimposed with test grids of equally spaced test points. The volume density of necrotic/inflamed adipose tissue in the rpAW-adipose tissue ($V_{V(Necrosis/rpAW)}$) was determined by point counting [31,32] as the quotient of the number of points hitting section areas of inflammation/necrosis within the rpAW-adipose tissue and the number of points hitting the rpAW-adipose tissue. Per case, 612 ± 58 points were counted. The total necrosis volume in the rpAW-adipose tissue ($V_{(Necrosis,\ rpAW)}$) was calculated by multiplication of $V_{V(Necrosis/rpAW)}$ with the total volume of the rpAW-adipose tissue ($V_{(rpAW)}$). The latter was calculated from the weight of the entire rpAW-fat depot and its tissue density [29].

2.11. Statistics

All data are presented as means ± SEM. For statistical analysis, longitudinal data for body weight, food intake, glucose and insulin levels during IVGTT were evaluated by ANOVA (Linear Mixed Models; SAS 8.2) taking the fixed effects of Group (obese vs. lean), Time (relative to glucose administration/feeding/treatment duration), and the interaction Group*Time into account. Data of body composition (DXA), clinical-chemical analyses, fasting glucose/insulin levels, HOMA-IR, organ weights/volumes and food digestibility were evaluated by ANOVA (General Linear Models; SAS 8.2) taking the fixed effects of Group, Time (= feeding duration) if applicable, and the interaction Group*Time into account. AUC insulin/glucose was calculated using GraphPad Prism® software (version 5.02). AUCs and all remaining

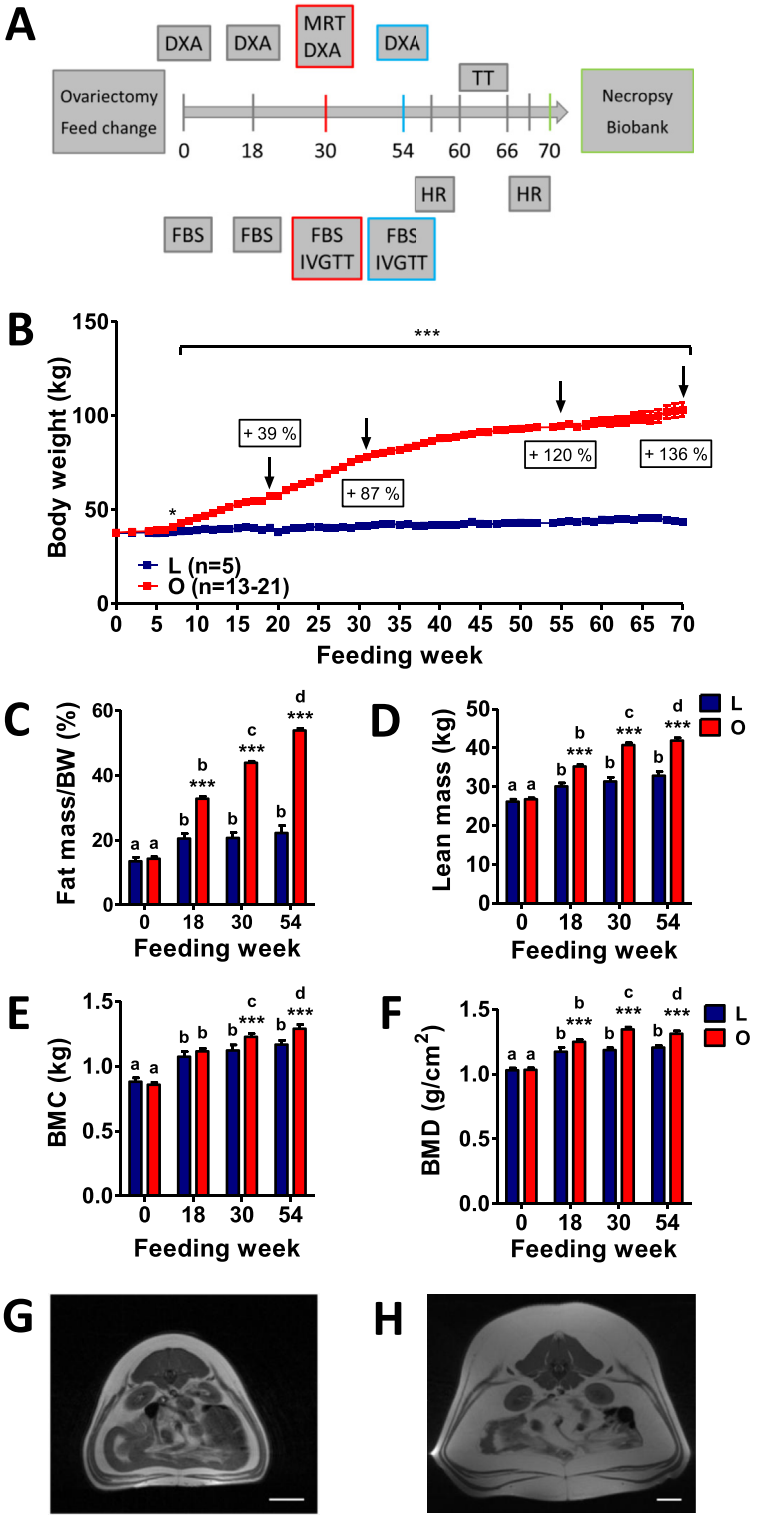

Figure 1: Study outline, body weight development, and body composition of Göttingen minipigs fed a HFHE-diet for 70 weeks. (A) Study outline**:** age of minipigs from the lean (L, n = 5) and obese group (O, n = 21) at the study start: 13 months, **FBS**: fasting blood sampling, **IVGTT:** intravenous glucose tolerance test, **HR**: heart rate, TT: treatment trial, **DXA**: dual-energy X-ray absorptiometry, **MRT**: magnetic resonance tomography. **(B)** Body weight gain of minipigs from the lean and obese group. **(C–F)** Body composition evaluated by DXA prior to HFHE-diet feeding (0) and at feeding week 18, 30 and 54, **(C)** Relative fat mass (%), **(D)** Absolute lean mass (kg), **(E)** Absolute bone mineral content (BMC, kg), **(F)** Bone mineral density (g/cm^2). **(G, H)** Representative MRT images of a lean **(G)** and an obese **(H)** minipig at the level of the kidneys showing subcutaneous and visceral obesity. Data are means ± SEM; *: $p<0.05$, **: $p<0.01$, ***: $p<0.001$. Significant differences within the groups are indicated by different letters, differences between lean and obese animals at the respective time point are indicated by asterisks.

parameters were tested for significance by Mann-Whitney-U-test or t-test using GraphPad Prism® software. If not indicated otherwise, p values less than 0.05 were considered significant.

3. RESULTS

3.1. HFHE-overfed Göttingen minipigs develop severe general obesity

Animals in the lean group (L-GM) received 3.1 ± 0.4 MJ DE/day (≙0.2 ± 0.03 MJ DE/kg $BW^{0.75}$) throughout the trial to maintain a lean body mass. Minipigs of the obese group (DIO-GM) consumed 10.8 ± 1.6 MJ DE/day (≙0.50 ± 0.07 MJ DE/kg $BW^{0.75}$) during the first (DI) and 51.1 ± 20.8 MJ DE/day (≙ 1.57 ± 0.55 MJ DE/kg $BW^{0.75}$) during the second (DII) diet digestibility test. The apparent digestibility (aD) of crude protein and nitrogen-free extracts (NfE) increased significantly with age (Suppl. Table 2; $p < 0.03$). The aD of all crude nutrients except crude fat (dry matter, crude protein, crude fiber, and NfE) was moderately but significantly higher in DIO-GM compared with L-GM (pairwise multiple comparison procedures). However, the aD of gross energy (GE) was not significantly different. The protein used in the diet was highly digestible throughout the trial (aD > 90%).

Prior to HFHE feeding, lean and obese minipigs were not significantly different in body weight (Figure 1B). After HFHE feeding, animals from the obese group constantly increased in body weight. At FW 18, 30, and 54, the body weights of DIO-GM were increased by 39%, 87%, and 120%, respectively, compared to age-matched L-GM. At the end of the study period (FW 70), the body weight of DIO-GM was increased by 136% relative to the age-matched L-GM (103.3 ± 3.7 vs. 43.6 ± 1.8 kg, $p < 0.0001$, Figure 1B).

Whole body DXA scans were performed prior to HFHE feeding as well as in FW 18, 30, and 54. While no significant differences were initially detected between the lean and obese groups, excessive HFHE feeding resulted in a constant and significant increase of total tissue (TT, Suppl. Figure 1A), fat mass (Figure 1C), lean mass (Figure 1D) and BMC (Figure 1E) in DIO-GM, while body composition of L-GM was maintained from week 18 onwards (Figure 1 & Suppl. Figure 1). Body composition of DIO-GM shifted towards fat mass (53.8% of TT at FW 54 in obese animals vs. 22.2% in lean animals; Figure 1C, Suppl. Figure 1B). MRT analyses at FW 30 revealed severe subcutaneous and visceral adiposity in DIO-GM (Figure 1G,H).

3.2. Obese Göttingen minipigs show an altered lipid profile

Prior to HFHE diet feeding, measures of clinical chemistry were comparable between the L-GM and DIO-GM minipigs (Suppl. Table 3). After 18 weeks of restricted HFHE feeding, L-GM showed significantly increased plasma total cholesterol and bilirubin concentrations, while iron concentration and alkaline phosphatase activity were decreased compared to the pre-feeding period (Figure 2A, Suppl. Table 3). DIO-GM showed pronounced alterations in lipid metabolism. Total cholesterol and triglyceride levels were significantly elevated at FW 18 and 30, but unaltered at FW 54 (Figure 2A,B). Plasma NEFA levels of DIO-GM were significantly increased at FW 54 (Figure 2C). Plasma levels of alanine-aminotransferase (ALT) were significantly reduced in DIO-GM vs. L-GM at FW 18, 30, and 54, while levels of aspartate-aminotransferase (AST) trended lower. Plasma levels of gamma-glutamyl transferase (GGT) were also significantly reduced at FW 54 (Suppl. Table 3). In addition, reduced plasma concentrations of total bilirubin and creatinine were observed in DIO-GM at FW 18 and 30. In contrast, plasma urea levels of DIO-GM were elevated at FW 18 and 30 (Suppl. Table 3).

3.3. Obese Göttingen minipigs reveal substantial hyperinsulinemia, insulin resistance and reduced glucose tolerance

DIO-GM had impaired glucose tolerance at FW 30 and 54 (13% and 39% higher AUC glucose than in L-GM; Figure 2D,E). Accordingly, glucose elimination rate was significantly decelerated at both time-points (Figure 2D,E). Fasting plasma glucose was significantly increased at FW 30 (Figure 2F), but remained within the reference range throughout the whole study period. Glucose-stimulated insulin secretion was markedly increased (79% and 175% increased AUC insulin compared to L-GM at FW 30 and 54, respectively; Figure 2G,H), resulting in significantly increased insulin:glucose ratios (Figure 2J,K). In addition, fasting insulin levels (Figure 2I) and HOMA-IR (Figure 2L) were significantly increased in DIO-GM at FW 30 and 54.

3.4. Increased heart rate in obese Göttingen minipigs at rest and during activity

Resting heart rate (beats per minute; bpm) was significantly elevated in DIO-GM compared to L-GM in FW 60 (96.9 ± 3.6 vs. 58.5 ± 4.8 bpm, $p = 0.0003$) and FW 69 (99.0 ± 4.2 vs. 66.9 ± 5.8 bpm, $p = 0.001$) (Suppl. Figure 2). After 1 min of relaxed walking, the heart rates of DIO-GM and L-GM increased to 147.7 ± 9.4 and 91.9 ± 4.4 bpm ($p = 0.007$), respectively, with peak levels of 175 ± 10.9 bpm and 107 ± 5.1 bpm in the two groups (Suppl. Figure 2).

3.5. DIO Göttingen minipigs show reduced food intake and weight reduction during short-term treatment with a GLP1R agonist

To examine the translatability of the DIO-GM model in regard to a pharmacological response, DIO-GM were treated for four weeks with a long-acting GLP1R agonist in an up-titration dosing regimen. The up-titration design (0.1 μg/kg BW for 20 days and 0.2 μg/kg BW for nine days) was employed to more mimic the dosing schedule in humans with liraglutide [33]. Treatment with the GLP1R agonist reduced daily food intake through the first two days relative to vehicle controls (Suppl. Figure 3A). Thereafter, daily food intake steadily increased and reached steady-state at treatment day 10 but was still significantly lower than in vehicle-treated DIO-GM (Suppl. Figure 3A). The dose increase to 0.2 μg/kg BW caused a more pronounced reduction in daily food intake compared to the initial dose. After treatment termination, daily food intake was normalized (Suppl. Figure 3A). By the end of this four-week study, DIO-GM treated with the GLP-1R agonist had a mean loss in BW of 1.5% from baseline while vehicle-treated DIO-GM had a mean BW gain of 4.6% ($p = 0.09$, Suppl. Figure 3B) from baseline. GLP1R agonist treatment did not cause significant changes in hematological and clinical-chemical parameters as determined at the end of the treatment trial (Suppl. Table 4).

3.6. Establishment of a biobank and pathomorphological alterations of adipose tissue

A biobank collection of samples of >20 different organs, tissues, and body fluids was established (Figure 3A), providing adequately processed specimen for a broad spectrum of subsequent analyses. This includes molecular analyses of RNA, proteins and metabolites, microbiomic analyses of intestinal contents, as well as qualitative and quantitative morphological study by light- and electron microscopy (details in Supplementary Table 7). DIO-GM displayed morbid obesity with massively enlarged subcutaneous and visceral fat tissue depots (Figure 3B,C). The proportion of subcutaneous and visceral fat in total fat was unaltered in DIO-GM compared to L-GM (data not shown). Apart from general obesity, DIO-GM consistently displayed a spectrum of morphological alterations. The most striking was the development of multifocal, severe adipose tissue inflammation and adipocyte necrosis in visceral abdominal adipose tissue depots (Figure 3D–L).

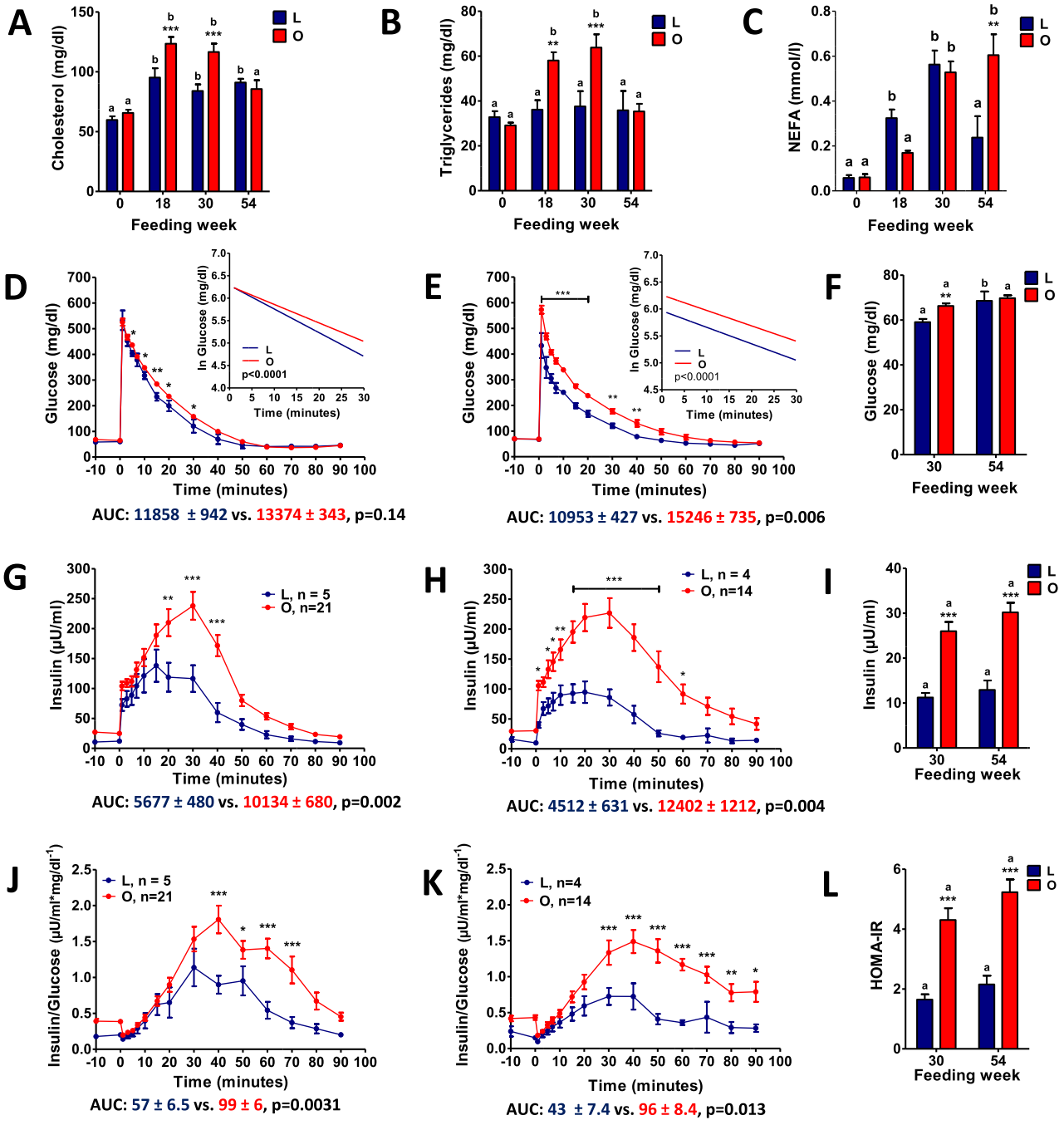

Figure 2: Fat metabolism and glucose control during IVGTT and insulin sensitivity in Göttingen minipigs fed a HFHE-diet for 70 weeks. Clinical-chemical analyses from plasma samples of lean (L) and obese (O) minipigs prior to HFHE-diet feeding (0) and at feeding week 18, 30 and 54; **(A)** Total cholesterol, **(B)** triglycerides, **(C)** non-esterified fatty acids (NEFA). **(D – L)** IVGTT from feeding week 30 **(D, G, J)** and 54 (E, H, K): Plasma glucose levels; the insert shows the net glucose elimination rate after glucose injection as calculated as the slope for the interval 1–30 min after glucose injection of the logarithmic transformation of the individual plasma glucose values **(D, E)**; Plasma insulin levels **(G, H)**; Insulin to glucose ratio **(J, K)**; Fasting glucose **(F)** and insulin **(I)** levels; HOMA-IR **(L)**. Data are means ± SEM; *: $p<0.05$, **: $p<0.01$, ***: $p<0.001$.

The volume density ($Vv_{(necrot.\ fat/total\ rpAW)}$) and total volume ($V_{(necrot.\ fat,\ total\ rpAW)}$) of necrotic fat tissue within the most affected abdominal retroperitoneal compartment was 8.7 ± 1.9% (range: 2–25%) and 178.5 ± 38.8 cm^3 in DIO-GM (Figure 3M). One animal within the DIO-GM group did not exhibit macroscopically identifiable areas of necrosis within the visceral adipose tissue. In histological sections, the profiles of adipocytes in rpAW of DIO-GM consistently appeared conspicuously larger than those of L-GM, as well as compared to the section profiles of subcutaneous adipocytes of both DIO-GM and L-GM (Figure 4A–F). Histopathological examination of samples from macroscopically altered and unaltered rpAW of DIO-GM revealed a spectrum of partially merging morphological findings, ranging from largely physiological (yet hypertrophic) fat cells, foci of acute single fat cell necrosis with moderate interstitial

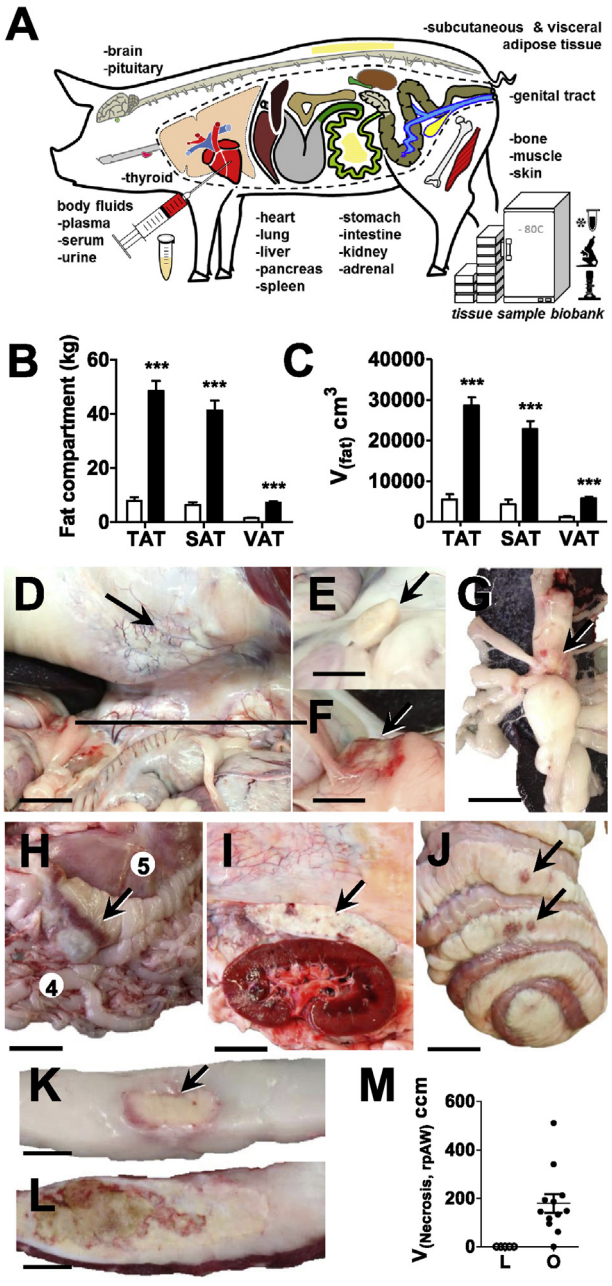

Figure 3: Biobank, macroscopic characteristics and quantitative-stereological analyses of fat tissue necroses in 3-year-old, ovariectomized Göttingen minipigs fed a HFHE-diet for 70 weeks. **(A):** Body fluids and tissues collected from lean (L) and obese (O) minipigs for the establishment of a biobank, see also Supplementary Table 7 for more detailed information; **(B, C)**: Mass **(B)** and total volumes **(C)** of different fat tissue compartments, TAT: total adipose tissue, SAT: subcutaneous adipose tissue, VAT: visceral adipose tissue; (**D**—**J**): Within the visceral adipose tissue, foci of fat tissue necrosis were most frequently observed in the following regions: **(D)** the retroperitoneal adipose tissue of the lateral abdominal wall (rpAW); view into the ventrally opened abdominal cavity. Note the white, dense areas of adipose tissue inflammation and necrosis in the retroperitoneal adipose tissue of the abdominal wall (arrow) and the fat tissue necrosis at the distal end of the splenic lobe of the pancreas lined by a hyperemic rim (line), bar = 6 cm; **(E,F)** the peri-pancreatic adipose tissue; unaltered morphology of the distal end of the pancreas' splenic lobe in a lean, need-based-fed minipig, bar = 3.5 cm **(E)** and detail enlargement of the peri-pancreatic fat tissue necrosis shown in **(F)**, bar = 3.5 cm; **(G)** the omental adipose tissue at the splenic hilus (arrow), bar = 2.5 cm and **(H)** the omental adipose tissue at the greater gastric curvature, bar = 7 cm; **(I)** the peri-renal retroperitoneal adipose tissue at the lateral abdominal wall (bar = 4 cm), and **(J)** less frequently in the jejunal and colonic mesentery, bar = 9 cm; **(K, L):** Detail enlargement of transverse sections of necrotic foci in the retroperitoneal fat tissue of the abdominal wall: areas of adipose tissue inflammation and necrosis in the visceral abdominal adipose tissue present as focally extensive, partially confluent, nodular, firm, white to yellow, dry, chalky, granular, and occasionally centrally liquefied foci of 0.5—20 cm in diameter, with ill-defined, irregularly shaped and hyperemic borders, Bars = 1 cm **(K)** and = 1.5 cm **(L)**; **(M):** Quantitative stereological analyses of necrotic/inflamed fat tissue areas in the retroperitoneal adipose tissue of the abdominal wall (rpAW), the mostly affected visceral fat tissue compartment; Total volume ($V_{(Necrosis,\ rpAW)}$) of fat tissue necrosis in retroperitoneal adipose tissue of the abdominal wall (rpAW). Data are means ± SEM.

lymphocytic infiltration, up to large areas with extensive fat cell necrosis, and severe chronic inflammatory cell infiltration of macrophages, multinucleate giant cells, and fewer neutrophils, lymphocytes, and plasma cells, accompanied by variable interstitial fibrosis, multifocal mineralization, and occasionally focal purulent liquefaction (Figure 4A—F). These alterations were particularly pronounced in the intra- and peripancreatic adipose tissue (Figure 4G,H). In contrast, adipose tissue inflammation and adipocyte necrosis was not observed in subcutaneous tissue of DIO-GM. Importantly, the subcutaneous and visceral fat tissue of L-GM did not show histopathological signs of inflammation or cell death.

In the liver of DIO-GM, multifocal hepatic foam-cell granulomas (accumulations of lipid-loaded macrophages, Figure 4I) were sporadically observed, whereas hepatocytic fat accumulation was only occasionally present while in skeletal muscles and the myocardium (Figure 4J) moderate interstitial lipidosis was observed.

In the terminal abdominal aorta and in cardiac coronary arteries of DIO-GM and L-GM, small, fatty, streak-like alterations were sporadically present while occlusive atherosclerotic lesions were not observed in any case (Suppl. Figure 5).

Throughout the observational period, eight minipigs had to be euthanized prior to the end of the study due to a severely decreased general condition associated with reduced food intake and dyspnea. Postmortem histopathological analyses showed substantial diffuse pulmonary lymphangiectasis and lymphatic lipidosis, as captured by IHC-detection of the lymphatic marker LYVE1 (lymphatic vessel endothelial hyaluronic acid receptor 1, Figure 4K, L).

4. DISCUSSION

To establish a large animal model for obesity research, we induced obesity by excessive feeding of a high-fat/high-energy diet (HFHE) in Göttingen minipigs, since this genetic background is frequently used in pharmaceutical research. Due to its relatively small size, compound testing in adult, obese animals is facilitated compared to domestic pig breeds considering handling and costs. A special HFHE diet was designed based on the fat, carbohydrate and protein sources and content used for a well-characterized DIO mouse model [22,23]. This enables comparative obesity studies between the two species.

Munich DIO-GM displayed crucial hallmarks of the metabolic syndrome, such as subcutaneous and visceral obesity, dyslipidemia, impaired glucose tolerance, fasting hyperinsulinemia and insulin resistance. The degree of obesity (44% and 54% mean total fat mass/body weight at FW 30 and 54 respectively) is in the same range as in women with advanced (>40% body fat) or morbid (>50% body fat) obesity [34]. Accordingly, the increased body weight of DIO-GM resulted preferentially from accumulation of fat mass (11-fold higher than in L-GM), whereas lean mass was only 1.6-fold increased, underlining the propensity of minipigs for obesity [35]. With increasing body weight and obesity DIO-GM showed a stepwise decrease in

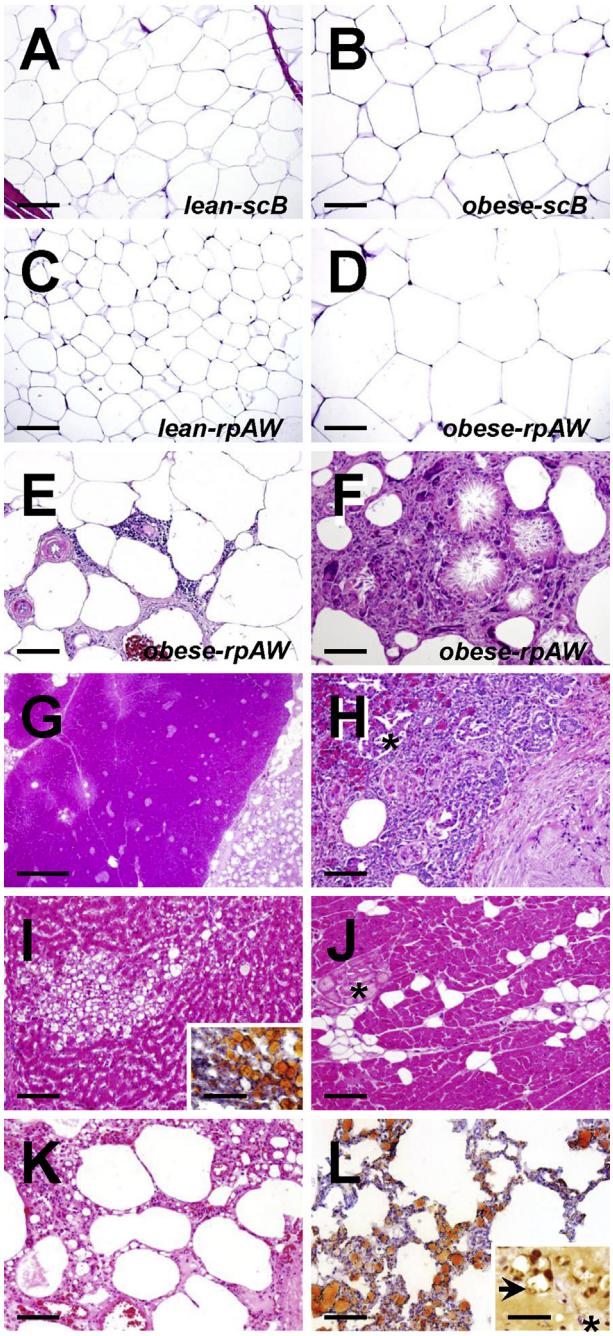

Figure 4: Histopathological findings in 3-year-old, ovariectomized Göttingen minipigs fed a HFHE-diet for 70 weeks. HE-stained paraffin-sections (**A**–**K**); Oil-red stained cryo-sections (**L** and inset to **I**). **A**–**D**: Histomorphology of unaltered subcutaneous adipose tissue of the back (***scB*** **A**, **B**) and of retroperitoneal adipose tissue of the lateral abdominal wall (***rpAW***, **C**, **D**) of lean, need-based HFHE-fed control pigs and obese HFHE-fed pigs without evident inflammatory or necrotic alterations. Note the drastically increased section profile areas of retroperitoneal adipocytes in obese pigs (**D**). Bars = 100 μm. **E**, **F**: Necrotic and inflammatory alterations in the retroperitoneal adipose tissue of obese HFHED-fed pigs. Bars = 100 μm. **E**: Moderate interstitial, perivascular lymphocytic infiltration, edema, hypertrophy of vascular walls and capillary endothelia, focal hemorrhage, and mild interstitial fibrosis. **F**: Extensive fat cell necrosis with saponification, cholesterol-crystal formation, and severe granulomatous inflammation (macrophages and numerous multinucleate giant cells). **G**–**L**: Visceral organ lesions in obese HFHED-fed pigs. **G**, **H**: Pancreas. **G**: Severe peri-pancreatic necrosis of fat (right side). Bar = 1 mm. **H**: Detail enlargement, illustrating the loss of acinar exocrine pancreatic parenchyma with (regenerative) proliferation of pancreatic duct epithelia adjacent to an area of fat tissue necrosis (right side). Asterisk marks the section profile of an endocrine pancreatic islet. Bar = 100 μm. **I**: Hepatic foam cell granuloma of lipid-loaded macrophages. **Inset to I**: Positive fat staining (oil-red, fat stains orange-red) in a cryo-section of liver tissue. Bars = 100 μm. **J**: Myocardial interstitial lipomatosis. Asterisk: Myocardial Purkinje-cells. Bars = 100 μm. **K**–**L**: Pulmonary lymphangiectasia and lipidosis. Bar = 100 μm. **L**: Positive fat-staining (oil-red, fat stains orange-red) in a cryo-section of lung tissue. **Inset to L**: Immunohistochemical detection (brown color) of LYVE1 (lymphatic marker). Asterisk: Blood capillary. Paraffin section. Chromogene: DAB. Nuclear counterstain: Hemalaun. Bar = 25 μm.

physical activity comparable to a sedentary lifestyle in humans. The resulting change in energy expenditure could be an additional trigger of excessive obesity and associated metabolic alterations.

Obese minipigs revealed a similar increase in the total volumes of subcutaneous (5.3-fold) and visceral fat tissue depots (4.9-fold), supporting the notion that fat distribution to visceral and subcutaneous depots is a heritable trait not altered by excessive weight gain [36,37]. Fat distribution to subcutaneous (80%) and visceral fat depots (20%) in L-GM and DIO-GM was comparable to lean [38] and obese humans [39]. In contrast, the proportion of visceral fat mass is substantially larger in lean (>40% of total fat mass) [40] and DIO mice (up to 70% of total fat mass) [41,42], which could be the reason for species-related physiological differences.

Diet digestibility tests confirmed a supply of all required nutrients in balanced amounts for lean and obese animals. The low apparent digestibility (aD) of fat was probably due to the fact that palm fat (stearin) was used in a refined form. The low aD of this major nutrient fraction also resulted in a reduced aD of dry matter and total energy. The moderate but significant increase of nutrient digestibility between the first and second balancing trial might be related to maturation of the animal's digestive physiology combined with an effect of habituation.

Obesity resulted in changes of multiple plasma metabolites. Compared with L-GM, plasma levels of total cholesterol and triglycerides were significantly increased in DIO-GM at FW 18 and 30, but unaltered at FW 54. This is most likely due to the lower daily energy intake (8 MJ ME) at FW 54 compared to 14 and 22 MJ ME at FW 18 and 30, respectively. In general, the total cholesterol pool is dependent on dietary intake, de novo synthesis, absorption efficiency, and excretion [43]. In contrast, fasting NEFA concentrations of DIO-GM were exclusively elevated in FW 54. This may be related to progressive deterioration of insulin sensitivity, as insulin is a potent inhibitor of lipolysis [44].

Plasma urea concentrations of DIO-GM were significantly increased in FW 18 and 30, but not different from L-GM at FW 54. This is most likely linked to the amount of dietary protein intake [45]. In addition, urea is a side-product of gluconeogenesis [46] that is physiologically inhibited by insulin. Progressive insulin resistance in DIO-GM may thus contribute to a higher urea production.

Interestingly, DIO-GM revealed significantly lower plasma creatinine levels than L-GM throughout the study. This is explained by the reduced relative lean mass of DIO-GM, as plasma creatinine levels correlate positively with muscle mass [47,48]. In addition, increased creatinine clearance was observed in obese humans [49,50].

By feeding the same diet to both L-GM and DIO-GM, metabolic consequences of obesity in comparison to normal weight can be evaluated in the absence of confounding effects due to different dietary components or distribution of energy sources within the diet. However, the change to fat as the dominant energy source resulted in changes (e.g. increase of total plasma cholesterol and bilirubin concentrations) in L-GM that have to be taken into account for the interpretation of data from DIO-GM (Figure 2A, Suppl. Table 3).

Analysis of glucose metabolism in obese (FW 30, mean fat mass 43.8%) and morbidly obese minipigs (FW 54, fat mass 53.8%) revealed reduced glucose tolerance combined with fasting and

stimulated hyperinsulinemia and increased HOMA-IR, indicative of an insulin-resistant state. Insulin sensitivity and glucose tolerance deteriorated with increasing obesity as indicated by increased AUC glucose, AUC insulin, and HOMA-IR despite of a lower glucose load during IVGTT (60% of glucose in FW 54 compared to FW 30). The association of insulin resistance and obesity is a well-known feature in humans [51]. Reduced glucose tolerance despite substantial hyperinsulinemia suggests some degree of decompensation as insulin secretion does not fully match the demand. Future clamp studies [52] using glucose tracers and evaluation of insulin clearance [53], an important additional modulator of plasma insulin concentration, will be used to characterize further glucose control in DIO-GM. Due to their size and blood volume, good compliance with training and the possibility of central arterial or venous catheter placement large animal models like pigs are more suitable for such studies [20].

Resting heart rate and heart rate during activity was found distinctly elevated in DIO-GM. Elevated resting heart rate is considered a risk factor for cardiovascular disease [54,55] and typically correlates with blood pressure [56]. Negative consequences of chronically increased heart rate/blood pressure as cardiac hypertrophy [57] were not observed in DIO-GM, however their heart weight was generally increased compared to L-GM.

The metabolic phenotype of the present DIO-GM model might have been triggered not only by HFHE-diet feeding and physical inactivity but also by ovariectomy. The lack of circulating estrogens is associated with increased food intake, reduced energy expenditure, increased body weight, and adiposity as well as altered body fat distribution and insulin resistance in animals and humans [58–61].

To validate this DIO-GM model for drug candidate testing, morbidly obese animals were treated with a long-acting GLP1R agonist previously tested in DIO mice [28]. A four-week treatment period distinctly reduced food intake and BW in ad libitum-fed DIO-GM. Positive effects on food intake and BW reduction were achieved using a much lower dose (up to 0.2 μg/kg BW = 0.02 mg per day) compared with the human dose of liraglutide (up to 3 mg per day) for obesity [33]. Similar to trials in humans, gastrointestinal adverse effects like nausea were present at the start but resolved within the first days of treatment. These data suggest similar positive effects of the GLP1R agonist in obese humans and pigs, although pigs seem to be more sensitive towards this class of drugs [62]. Long-term treatment trials can determine the peptide's full potency and efficacy on body weight gain, and metabolic parameters. Since pigs lack uncoupling protein 1 (UCP1) [63], evaluation of the GLP1R agonist's effect on uncoupled respiration/thermogenesis as has been described in mice and rats [64] may be more reflective of the human state where UCP1 levels are relatively low compared to mice [21].

A prominent finding in DIO-GM was multifocal, large-scale visceral adipose tissue inflammation and adipocyte necrosis, which was not previously described in this species. By contrast, subcutaneous adipose tissue was not affected. Obesity-associated adipose tissue inflammation has been described in rodents [65] and humans [17,66]. Despite a detailed knowledge of obesity-associated metabolic consequences, triggers and underlying mechanisms of adipose tissue inflammation as well as their causal relationships to comorbidities are uncertain [18]. Generally, extrinsic or intrinsic factors are potential triggers whereby intrinsic factors can originate from living or dying/dead adipocytes. Bacterial-derived lipopolysaccharides [67] entering the circulation due to increased obesity-associated gut-permeability [68], increased FFA concentrations [69,70] and the lack of estrogens [71] were linked to adipose tissue inflammation. Also, relative deficiency in vitamin E, a potent scavenger of reactive oxygen species (ROS), favoring (per)oxidative alteration of lipids and cell membranes with formation of free radicals has been discussed as trigger for fat tissue inflammation [72]. Furthermore, the interstitial release of active pancreatic lipolytic and proteolytic enzymes [73] might contribute to inflammation and necrosis as well as hypoxia due to vascular damage, compression, insufficient angiogenesis [74] or mechanical stress resulting in incorrect remodeling of WAT extracellular matrix (ECM) and impaired expansion of adipocytes [75,76].

The reason for exclusive observation of adipose tissue inflammation and necrosis in visceral adipose tissue depots of DIO-GM is currently unknown but indicates a generally increased susceptibility of severely hypertrophic retroperitoneal adipocytes to undergo necrosis possibly due to differences in compensatory mechanisms for increasing obesity, e.g. fat composition, remodeling processes, or vascularization.

For the evaluation of the pathogenic relevance of potential triggers of adipose tissue inflammation, underlying mechanisms and the multiorganic consequences of morbid obesity a biobank of selected tissues and body fluids from lean and obese minipigs was established. The focus was set on sampling of altered and unaltered adipose tissue from a large range of fat depots (subcutaneous: back, abdomen; visceral: abdominal subperitoneal, perirenal, mesenteric, omental). In this way, a unique resource was generated from adult minipigs that had undergone a serial metabolic characterization within an observation period of 70 weeks.

In conclusion, Munich DIO minipigs present the hallmarks of the metabolic syndrome with extensive adipose tissue inflammation. They constitute a valuable model for the evaluation of upstream triggers, underlying mechanisms and metabolic consequences of adipose tissue inflammation. They can serve as a valuable model for testing of novel drug candidates.

FUNDING

This study was supported by the German Center for Diabetes Research (DZD).

AUTHOR CONTRIBUTIONS

SR, AB, and EW designed the study. SR and EW wrote the manuscript. AB, BD, GD, TM, BF, CC, MB, IN, BR, SS, SZ, MR, AG, SH, MHA, RW, EK, AS, RDM, MR, and MT contributed to discussions and edited and reviewed the manuscript. SR, GD, IN and SS did the metabolic characterization of the DIO minipigs and treatment trial. GD and MR performed training of DIO minipigs. BD generated the HFHE diet and performed balancing trials. MB and AS performed DXA and MRT scans. BR, AG, and SH did clinical chemical analyses. BF and RDM generated the GLP1 receptor agonist. AB, SR, GD, and SS performed necropsies. SR and EW are the guarantors of this work and, as such, had full access to all the data in the study and take responsibility for the integrity of the data and the accuracy of the data analysis. SR, AB, BD, and EW analyzed the data.

ACKNOWLEDGMENTS

The authors thank Andrea Bähr, Pauline Deffner, Stefanie Egerer, Lina Fonteyne, Sebastian Fröhlich, Sophie Gumbert, Arne Hinrichs, Melanie Janda, Barbara Kessler, Roland Maurer, Sophia Mück, Simon Reiter, and Christina Söckler for excellent assistance with tissue harvesting at necropsy and care of the animals and Sepp Bichler, Christina Blechinger, Ebru Brockhaus, Sven Brockhaus, Gilio Cafiero, Sebastian Cucuruz, Christian Erdle, Adrian Frille, Bärbel Garner, Marold Handl, Sebastian Kaidel, Harald Paul, and Lisa Pichl for excellent technical assistance and Christina Blechinger for excellent assistance with necropsy preparation and coordination.

CONFLICT OF INTEREST

No potential conflicts of interest relevant to this article were reported.

APPENDIX A. SUPPLEMENTARY DATA

Supplementary data related to this article can be found at https://doi.org/10.1016/j.molmet.2018.06.015.

REFERENCES

[1] Afshin, A., Forouzanfar, M.H., Reitsma, M.B., Sur, P., Estep, K., Lee, A., et al., 2017. Health effects of overweight and obesity in 195 countries over 25 years. New England Journal of Medicine 377:13–27.

[2] Kahn, B.B., Flier, J.S., 2000. Obesity and insulin resistance. Journal of Clinical Investigation 106:473–481.

[3] Williams, P.T., Krauss, R.M., 1997. Associations of age, adiposity, menopause, and alcohol intake with low-density lipoprotein subclasses. Arteriosclerosis, Thrombosis, and Vascular Biology 17:1082–1090.

[4] Head, G.A., Lim, K., Barzel, B., Burke, S.L., Davern, P.J., 2014. Central nervous system dysfunction in obesity-induced hypertension. Current Hypertension Reports 16:466.

[5] Hu, Y., Bhupathiraju, S.N., de Koning, L., Hu, F.B., 2014. Duration of obesity and overweight and risk of type 2 diabetes among US women. Obesity (Silver Spring) 22:2267–2273.

[6] Fabbrini, E., Sullivan, S., Klein, S., 2010. Obesity and nonalcoholic fatty liver disease: biochemical, metabolic, and clinical implications. Hepatology 51:679–689.

[7] Beuther, D.A., Sutherland, E.R., 2007. Overweight, obesity, and incident asthma: a meta-analysis of prospective epidemiologic studies. American Journal of Respiratory and Critical Care Medicine 175:661–666.

[8] Ligibel, J.A., Alfano, C.M., Courneya, K.S., Demark-Wahnefried, W., Burger, R.A., Chlebowski, R.T., et al., 2014. American Society of Clinical Oncology position statement on obesity and cancer. Journal of Clinical Oncology 32:3568–3574.

[9] Van Gaal, L.F., Mertens, I.L., De Block, C.E., 2006. Mechanisms linking obesity with cardiovascular disease. Nature 444:875–880.

[10] Hassing, L.B., Dahl, A.K., Thorvaldsson, V., Berg, S., Gatz, M., Pedersen, N.L., et al., 2009. Overweight in midlife and risk of dementia: a 40-year follow-up study. International Journal of Obesity 33:893–898.

[11] Federation, I.D., 2006. The IDF consensus worldwide definition of the metabolic syndrome. In: IDF communications, Brussels, Belgium.

[12] Montani, J.P., Carroll, J.F., Dwyer, T.M., Antic, V., Yang, Z., Dulloo, A.G., 2004. Ectopic fat storage in heart, blood vessels and kidneys in the pathogenesis of cardiovascular diseases. International Journal of Obesity and Related Metabolic Disorders 28(Suppl. 4):S58–S65.

[13] Tchkonia, T., Thomou, T., Zhu, Y., Karagiannides, I., Pothoulakis, C., Jensen, M.D., et al., 2013. Mechanisms and metabolic implications of regional differences among fat depots. Cell Metabolism 17:644–656.

[14] Ouchi, N., Parker, J.L., Lugus, J.J., Walsh, K., 2011. Adipokines in inflammation and metabolic disease. Nature Reviews Immunology 11:85–97.

[15] Wernstedt Asterholm, I., Tao, C., Morley, T.S., Wang, Q.A., Delgado-Lopez, F., Wang, Z.V., et al., 2014. Adipocyte inflammation is essential for healthy adipose tissue expansion and remodeling. Cell Metabolism 20:103–118.

[16] Sun, K., Tordjman, J., Clement, K., Scherer, P.E., 2013. Fibrosis and adipose tissue dysfunction. Cell Metabolism 18:470–477.

[17] Divoux, A., Tordjman, J., Lacasa, D., Veyrie, N., Hugol, D., Aissat, A., et al., 2010. Fibrosis in human adipose tissue: composition, distribution, and link with lipid metabolism and fat mass loss. Diabetes 59:2817–2825.

[18] Reilly, S.M., Saltiel, A.R., 2017. Adapting to obesity with adipose tissue inflammation. Nature Reviews Endocrinology 13:633–643.

[19] Heydemann, A., 2016. An overview of murine high fat diet as a model for type 2 diabetes mellitus. J Diabetes Res 2016:2902351.

[20] Kleinert, M., Clemmensen, C., Hofmann, S.M., Moore, M.C., Renner, S., Woods, S.C., et al., 2018. Animal models of obesity and diabetes mellitus. Nature Reviews Endocrinology 14:140–162.

[21] Renner, S., Dobenecker, B., Blutke, A., Zols, S., Wanke, R., Ritzmann, M., et al., 2016. Comparative aspects of rodent and nonrodent animal models for mechanistic and translational diabetes research. Theriogenology 86:406–421.

[22] Clemmensen, C., Finan, B., Fischer, K., Tom, R.Z., Legutko, B., Sehrer, L., et al., 2015. Dual melanocortin-4 receptor and GLP-1 receptor agonism amplifies metabolic benefits in diet-induced obese mice. EMBO Molecular Medicine 7:288–298.

[23] Muller, T.D., Sullivan, L.M., Habegger, K., Yi, C.X., Kabra, D., Grant, E., et al., 2012. Restoration of leptin responsiveness in diet-induced obese mice using an optimized leptin analog in combination with exendin-4 or FGF21. Journal of Peptide Science 18:383–393.

[24] Kamphues, J., 2014. Supplemente zur Tierernährung für Studium und Praxis. Hannover, Germany: Schlütersche.

[25] Kremer, P.V., Fernandez-Figares, I., Forster, M., Scholz, A.M., 2012. In vivo body composition in autochthonous and conventional pig breeding groups by dual-energy X-ray absorptiometry and magnetic resonance imaging under special consideration of Cerdo Iberico. Animal 6:2041–2047.

[26] Kremer, P.V., Forster, M., Scholz, A.M., 2013. Use of magnetic resonance imaging to predict the body composition of pigs in vivo. Animal 7:879–884.

[27] Renner, S., Fehlings, C., Herbach, N., Hofmann, A., von Waldthausen, D.C., Kessler, B., et al., 2010. Glucose intolerance and reduced proliferation of pancreatic beta-cells in transgenic pigs with impaired glucose-dependent insulinotropic polypeptide function. Diabetes 59:1228–1238.

[28] Finan, B., Yang, B., Ottaway, N., Smiley, D.L., Ma, T., Clemmensen, C., et al., 2015. A rationally designed monomeric peptide triagonist corrects obesity and diabetes in rodents. Nature Medicine 21:27–36.

[29] Albl, B., Haesner, S., Braun-Reichhart, C., Streckel, E., Renner, S., Seeliger, F., et al., 2016. Tissue sampling guides for porcine biomedical models. Toxicologic Pathology 44:414–420.

[30] Scherle, W., 1970. A simple method for volumetry of organs in quantitative stereology. Mikroskopie 26:57–60.

[31] Blutke, A., Schneider, M.R., Wolf, E., Wanke, R., 2016. Growth hormone (GH)-transgenic insulin-like growth factor 1 (IGF1)-deficient mice allow dissociation of excess GH and IGF1 effects on glomerular and tubular growth. Physiol Rep 4 e12709.

[32] Howard, C.V., Reed, M.G., 2005. Unbiased stereology. New York: BIOS Scientific Publishers.

[33] Mehta, A., Marso, S.P., Neeland, I.J., 2017. Liraglutide for weight management: a critical review of the evidence. Obes Sci Pract 3:3–14.

[34] Gallagher, D., Heymsfield, S.B., Heo, M., Jebb, S.A., Murgatroyd, P.R., Sakamoto, Y., 2000. Healthy percentage body fat ranges: an approach for developing guidelines based on body mass index. American Journal of Clinical Nutrition 72:694–701.

[35] Dyson, M.C., Alloosh, M., Vuchetich, J.P., Mokelke, E.A., Sturek, M., 2006. Components of metabolic syndrome and coronary artery disease in female Ossabaw swine fed excess atherogenic diet. Comparative Medicine 56:35–45.

[36] Fox, C.S., Liu, Y., White, C.C., Feitosa, M., Smith, A.V., Heard-Costa, N., et al., 2012. Genome-wide association for abdominal subcutaneous and visceral adipose reveals a novel locus for visceral fat in women. PLoS Genetics 8:e1002695.

[37] Fox, C.S., White, C.C., Lohman, K., Heard-Costa, N., Cohen, P., Zhang, Y., et al., 2012. Genome-wide association of pericardial fat identifies a unique locus for ectopic fat. PLoS Genetics 8:e1002705.

[38] Frayn, K.N., Karpe, F., 2014. Regulation of human subcutaneous adipose tissue blood flow. International Journal of Obesity (Lond) 38:1019–1026.

[39] Linder, K., Springer, F., Machann, J., Schick, F., Fritsche, A., Haring, H.U., et al., 2014. Relationships of body composition and liver fat content with

insulin resistance in obesity-matched adolescents and adults. Obesity (Silver Spring) 22:1325–1331.
[40] Papademetris, X., Shkarin, P., Staib, L.H., Behar, K.L., 2005. Regional whole body fat quantification in mice. Inf Process Med Imaging 19:369–380.
[41] Foster, M.T., Softic, S., Caldwell, J., Kohli, R., de Kloet, A.D., Seeley, R.J., 2013. Subcutaneous adipose tissue transplantation in diet-induced obese mice attenuates metabolic dysregulation while removal exacerbates it. Physics Reports 1: e00015.
[42] Kahle, M., Horsch, M., Fridrich, B., Seelig, A., Schultheiss, J., Leonhardt, J., et al., 2013. Phenotypic comparison of common mouse strains developing high-fat diet-induced hepatosteatosis. Molecular Metabolism 2:435–446.
[43] Griffin, J.D., Lichtenstein, A.H., 2013. Dietary cholesterol and plasma lipoprotein profiles: randomized-controlled trials. Current Nutrition Reports 2: 274–282.
[44] Chakrabarti, P., Kim, J.Y., Singh, M., Shin, Y.K., Kim, J., Kumbrink, J., et al., 2013. Insulin inhibits lipolysis in adipocytes via the evolutionarily conserved mTORC1-Egr1-ATGL-mediated pathway. Molecular and Cellular Biology 33: 3659–3666.
[45] Bassily, N.S., Michael, K.G., Said, A.K., 1982. Blood urea content for evaluating dietary protein quality. Nahrung 26:759–764.
[46] Schutz, Y., 2011. Protein turnover, ureagenesis and gluconeogenesis. International Journal for Vitamin and Nutrition Research 81:101–107.
[47] Baxmann, A.C., Ahmed, M.S., Marques, N.C., Menon, V.B., Pereira, A.B., Kirsztajn, G.M., et al., 2008. Influence of muscle mass and physical activity on serum and urinary creatinine and serum cystatin C. Clinical Journal of the American Society of Nephrology 3:348–354.
[48] Schutte, J.E., Longhurst, J.C., Gaffney, F.A., Bastian, B.C., Blomqvist, C.G., 1981. Total plasma creatinine: an accurate measure of total striated muscle mass. Journal of Applied Physiology, Respiratory, Environmental & Exercise Physiology 51:762–766.
[49] Gerchman, F., Tong, J., Utzschneider, K.M., Zraika, S., Udayasankar, J., McNeely, M.J., et al., 2009. Body mass index is associated with increased creatinine clearance by a mechanism independent of body fat distribution. Journal of Clinical Endocrinology & Metabolism 94:3781–3788.
[50] Helal, I., Fick-Brosnahan, G.M., Reed-Gitomer, B., Schrier, R.W., 2012. Glomerular hyperfiltration: definitions, mechanisms and clinical implications. Nature Reviews Nephrology 8:293–300.
[51] Czech, M.P., 2017. Insulin action and resistance in obesity and type 2 diabetes. Nature Medicine 23:804–814.
[52] Kim, J.K., 2009. Hyperinsulinemic–euglycemic clamp to assess insulin sensitivity in vivo. In: Stocker, C. (Ed.), Type 2 diabetes. Humana Press.
[53] Polidori, D.C., Bergman, R.N., Chung, S.T., Sumner, A.E., 2016. Hepatic and extrahepatic insulin clearance are differentially regulated: results from a novel model-based analysis of intravenous glucose tolerance data. Diabetes 65: 1556–1564.
[54] Cook, S., Togni, M., Schaub, M.C., Wenaweser, P., Hess, O.M., 2006. High heart rate: a cardiovascular risk factor? European Heart Journal 27:2387–2393.
[55] Bohm, M., Reil, J.C., Deedwania, P., Kim, J.B., Borer, J.S., 2015. Resting heart rate: risk indicator and emerging risk factor in cardiovascular disease. The American Journal of Medicine 128:219–228.
[56] Christofaro, D.G.D., Casonatto, J., Vanderlei, L.C.M., Cucato, G.G., Dias, R.M.R., 2017. Relationship between resting heart rate, blood pressure and pulse pressure in adolescents. Arquivos Brasileiros de Cardiologia 108: 405–410.
[57] Lavie, C.J., Arena, R., Alpert, M.A., Milani, R.V., Ventura, H.O., 2018. Management of cardiovascular diseases in patients with obesity. Nature Reviews Cardiology 15:45–56.
[58] Carr, M.C., 2003. The emergence of the metabolic syndrome with menopause. Journal of Clinical Endocrinology & Metabolism 88:2404–2411.
[59] Christoffersen, B.O., Gade, L.P., Golozoubova, V., Svendsen, O., Raun, K., 2010. Influence of castration-induced testosterone and estradiol deficiency on obesity and glucose metabolism in male Gottingen minipigs. Steroids 75: 676–684.
[60] Heine, P.A., Taylor, J.A., Iwamoto, G.A., Lubahn, D.B., Cooke, P.S., 2000. Increased adipose tissue in male and female estrogen receptor-alpha knockout mice. Proceedings of the National Academy of Sciences of the U S A 97:12729–12734.
[61] Wallen, W.J., Belanger, M.P., Wittnich, C., 2001. Sex hormones and the selective estrogen receptor modulator tamoxifen modulate weekly body weights and food intakes in adolescent and adult rats. Journal of Nutrition 131:2351–2357.
[62] Streckel, E., Braun-Reichhart, C., Herbach, N., Dahlhoff, M., Kessler, B., Blutke, A., et al., 2015. Effects of the glucagon-like peptide-1 receptor agonist liraglutide in juvenile transgenic pigs modeling a pre-diabetic condition. Journal of Translational Medicine 13:73.
[63] Jastroch, M., Andersson, L., 2015. When pigs fly, UCP1 makes heat. Molecular Metabolism 4:359–362.
[64] Beiroa, D., Imbernon, M., Gallego, R., Senra, A., Herranz, D., Villarroya, F., et al., 2014. GLP-1 agonism stimulates brown adipose tissue thermogenesis and browning through hypothalamic AMPK. Diabetes 63:3346–3358.
[65] Cinti, S., Mitchell, G., Barbatelli, G., Murano, I., Ceresi, E., Faloia, E., et al., 2005. Adipocyte death defines macrophage localization and function in adipose tissue of obese mice and humans. The Journal of Lipid Research 46: 2347–2355.
[66] Lumeng, C.N., Saltiel, A.R., 2011. Inflammatory links between obesity and metabolic disease. Journal of Clinical Investigation 121:2111–2117.
[67] Saad, M.J., Santos, A., Prada, P.O., 2016. Linking gut microbiota and inflammation to obesity and insulin resistance. Physiology (Bethesda) 31: 283–293.
[68] Lam, Y.Y., Ha, C.W., Campbell, C.R., Mitchell, A.J., Dinudom, A., Oscarsson, J., et al., 2012. Increased gut permeability and microbiota change associate with mesenteric fat inflammation and metabolic dysfunction in diet-induced obese mice. PLoS One 7:e34233.
[69] Makowski, L., Brittingham, K.C., Reynolds, J.M., Suttles, J., Hotamisligil, G.S., 2005. The fatty acid-binding protein, aP2, coordinates macrophage cholesterol trafficking and inflammatory activity. Macrophage expression of aP2 impacts peroxisome proliferator-activated receptor gamma and IkappaB kinase activities. Journal of Biological Chemistry 280:12888–12895.
[70] Vitseva, O.I., Tanriverdi, K., Tchkonia, T.T., Kirkland, J.L., McDonnell, M.E., Apovian, C.M., et al., 2008. Inducible Toll-like receptor and NF-kappaB regulatory pathway expression in human adipose tissue. Obesity (Silver Spring) 16:932–937.
[71] Shen, M., Kumar, S.P., Shi, H., 2014. Estradiol regulates insulin signaling and inflammation in adipose tissue. Hormone Molecular Biology and Clinical Investigation 17:99–107.
[72] Alcala, M., Sanchez-Vera, I., Sevillano, J., Herrero, L., Serra, D., Ramos, M.P., et al., 2015. Vitamin E reduces adipose tissue fibrosis, inflammation, and oxidative stress and improves metabolic profile in obesity. Obesity (Silver Spring) 23:1598–1606.
[73] Aho, H.J., Sternby, B., Nevalainen, T.J., 1986. Fat necrosis in human acute pancreatitis. An immunohistological study. Acta Pathologica Microbiologica et Immunologica Scandinavica A 94:101–105.
[74] Lijnen, H.R., 2008. Angiogenesis and obesity. Cardiovascular Research 78: 286–293.
[75] Henegar, C., Tordjman, J., Achard, V., Lacasa, D., Cremer, I., Guerre-Millo, M., et al., 2008. Adipose tissue transcriptomic signature highlights the pathological relevance of extracellular matrix in human obesity. Genome Biology 9:R14.
[76] Wynn, T.A., 2007. Common and unique mechanisms regulate fibrosis in various fibroproliferative diseases. Journal of Clinical Investigation 117: 524–529.

